Available online at www.sciencedirect.com
SCIENCE DIRECT
Journal of Geodynamics 41 (2006) 77–86
JOURNAL OF GEODYNAMICS
http://www.elsevier.com/locate/jog

Kinematic and static GPS techniques for estimating tidal displacements with application to Antarctica

Matt King *

School of Civil Engineering and Geosciences, University of Newcastle, Newcastle upon Tyne NE1 7RU, United Kingdom

Accepted 30 August 2005

Abstract

For several decades relative gravimetric measurements have allowed the precise observation of harmonic signals related to Earth body and ocean tides. More recently, GPS data have been shown to be precise enough to allow the determination of antenna displacements at tidal frequencies in three dimensions. In this paper I focus on a comparison between 'kinematic' and 'static' tidal displacement estimation techniques using GPS data between ∼1998.5 and 2003.5 from South Pole (AMUN). The GPS estimates are compared with modelled values using the TPXO.6 and FES99 numerical tide models which themselves are found to be in agreement at the ∼1/100 mm level except for O_1 and N_2. The kinematic estimates are of lower accuracy to the static estimates and the height time series is dominated by non-tidal errors. The best resolved frequencies in the kinematic analysis are solar-related constituents, suggesting the presence of GPS systematic biases. The static analysis agrees with the model estimates, generally at the sub-mm level, with larger errors evident at S_2, K_1 and K_2 frequencies. A time-variable behaviour of K_2 is demonstrated. After combination of all daily data, high correlations (0.7–0.9) are evident between north and east components of each constituent, whilst the remainder of the correlations are less than 0.06. These correlations alter with site latitude and point to the source of the correlations being related to the non-integer ambiguities in the daily GPS estimates which are known to introduce correlations between horizontal and vertical site coordinate components and also change with site latitude. Fixing carrier phase ambiguities to integers may therefore increase the precision of harmonic parameter estimates using GPS.

Keywords: Ocean tide loading displacements; Static and kinematic GPS; South Pole

1. Introduction

Relative gravimetry currently represents the most accurate measurement technique for the estimation of loading variations due to tidal mass redistribution, with ongoing improvements through the use of new technologies (Hinderer and Crossley, 2004). Alternatively, ocean tide loading displacements may be determined using Very Long Baseline Interferometry (VLBI) observations with sub-mm accuracies in three dimensions (Petrov and Ma, 2003; Schuh and Moehlmann, 1989; Sovers, 1994). However, due to logistical and cost restrictions there are only ∼50–100 sites where either VLBI or long-term gravimetric measurements are available. Consequently there are many locations where tidal measurements are not being made at present to, for example, validate ocean tide models.

* Tel.: +44 191 222 7833; fax: +44 191 222 6502.
E-mail address: m.a.king@ncl.ac.uk.

0264-3707/$ – see front matter © 2005 Elsevier Ltd. All rights reserved.
doi:10.1016/j.jog.2005.08.019

Recently, it has been demonstrated that GPS data may be used to estimate semi-diurnal and diurnal tidal loading displacements with accuracies in each of three dimensions of ∼0.5–5.0 mm (Allinson et al., 2004; Khan and Scherneck, 2003; Khan and Tscherning, 2001). The global GPS network, including the network of the International GPS Service, now consists of several thousand sites and offers the possibility of much greater spatial density of tidal loading displacement measurements made on a continuous basis (unlike VLBI). Tidal displacements at these sites are also of interest since any mismodelled tidal signal will propagate into longer period signals (Lambert et al., 1998; Penna and Stewart, 2003) and bias estimates of tropospheric water vapour (Vey et al., 2002). Importantly, GPS, like VLBI, does not require regular calibration and hence long time series of data may be collected with little manual intervention. These space geodetic techniques are also not sensitive to local mass variations and hence may be located at any distance from the coast. The main disadvantage of GPS measurements of this type is the satellite orbital period and constellation repeat period is at K_2 and K_1 periods, respectively, meaning that systematic errors are prone to map into tidal displacement estimates at these frequencies and their higher order harmonics.

To date, GPS-based studies have concentrated on the determination of diurnal and semi-diurnal parameters, typically the four major diurnal constituents (K_1, O_1, P_1, Q_1) and the four major semi-diurnal constituents (M_2, S_2, N_2, K_2). Two main techniques have been applied: (i) generation of sub-daily GPS coordinate time series after which a conventional tidal analysis is performed (Vey et al., 2002) or (ii) explicit parameterisation at the required frequencies at the static GPS data processing stage on a daily basis followed by combination (Allinson et al., 2004; Schenewerk et al., 2001). Generally the first technique uses 1–4 h batch coordinate solutions, and if horizontal displacements are to be estimated ambiguity parameters must be fixed to integer values to avoid aliasing of vertical signals into the horizontal estimates (King et al., 2003). However, this requirement to fix ambiguities does not apply when coordinates are derived every measurement epoch (i.e., in a kinematic solution). However, the accuracy of kinematic GPS solutions using long time series of onshore data are yet to be demonstrated, although ocean tide measurements have been made using a kinematic Precise Point Positioning (PPP) approach (King and Aoki, 2003) suggesting that this approach may be feasible.

In this paper I compare tidal loading displacement estimates using both the kinematic and static technique using GPS data collected between ∼1998.5 and 2003.5 at the South Pole (−89.9978°S, 139.1822°E, ∼250 m from the Pole), hereafter referred to by its GPS site name, AMUN. The site moves in a northerly direction at the velocity of the ice it is attached to, which is approximately 9.98 m year^{-1}. This site is of specific interest since diurnal and semi-diurnal Earth body tides are theoretically zero at the Poles (Agnew, 1995; Knopoff et al., 1989), and are ≪0.1 mm at AMUN. Ocean tide loading displacements do not exceed ∼2 mm at this site, allowing a test on the accuracy of tidal displacement measurements using GPS at different tidal frequencies. A near-perfectly symmetric GPS satellite constellation exists at AMUN, meaning assessment of the measurement techniques may be made while several potential sources of error are eliminated. However, observations are limited to satellites at low elevation angles due to the satellite orbital inclination, reducing the geometric strength of the solution and tropospheric conditions are not be typical (on a global scale) due to the extremely dry atmosphere in Antarctica.

The major semi-diurnal, diurnal and fortnightly constituents were each estimated and the results compared with modelled ocean tide loading displacement measurements from several recent ocean tide models using the SPOTL software (Agnew, 1997). I also show the effect of time-variable K_2 errors in the static approach and discuss methods for mitigating their effect on the other constituents and the impact of ambiguity resolution on the static solutions.

2. Diurnal and semi-diurnal signals

2.1. Model estimates

Ocean tide loading displacements were computed using the SPOTL software. Until recent years the Antarctic coastline has been poorly determined (e.g., Fricker et al., 2001), and consequently the care taken by D. Agnew to include an up-to-date Antarctic coastline in SPOTL is important. Estimates from two recent models were computed, namely TPXO.6 (Egbert et al., 1994; Egbert and Erofeeva, 2002) and FES99 (Lefevre et al., 2002), and these are shown in Tables 1–3. P_1 is not included in FES99 and hence it is not shown. Agnew (1995) showed that a predecessor of FES99, FES95.2, was at the time the most accurate model for AMUN when compared against the relative gravity record there. Comparison of these more recent models with the same gravity analysis results (Knopoff et al., 1989) show these models to be in closer agreement with the gravity measurements than FES95.2 (King et al., 2005). The

Table 1
Estimates of AMUN vertical site displacement amplitude (first, in mm) and phase (second, in degrees) based on the TPXO.6 and FES99 models and GPS data

Method	Constituent (vertical)							
	M_2	S_2	N_2	K_2	K_1	O_1	P_1	Q_1
TPXO.6	1.11, 28.6	0.11, 51.2	0.46, −16.7	0.05, 94.7	1.10, −13.8	0.77, −104.1	0.41, −6.8	0.14, −147.4
FES99	1.11, 30.6	0.09, 133.1	0.21, −24.2	0.06, 114.8	1.10, −11.6	0.57, −117.3	–	0.18, −153.9
Kinematic	0.2 ± 0.1, −8.3	0.3 ± 0.1, 56.7	0.1 ± 0.1, 23.3	0.6 ± 0.1, 61.6	2.3 ± 0.2, 30.2	0.4 ± 0.2, 118.2	0.9 ± 0.3, 7.4	0.1 ± 0.2, 107.7
Static	1.9 ± 1.2, 22.5	1.5 ± 1.2, −10.8	0.8 ± 1.2, −33.3	3.3 ± 1.2, 83.4	4.0 ± 1.3, 33.1	1.4 ± 1.3, −99.1	2.0 ± 1.3, −7.4	0.6 ± 1.3, −164.1
Static + PN	1.5 ± 1.3, 26.8	2.1 ± 1.5, −8.7	0.5 ± 1.3, −22.8	8.7 ± 7.8, 99.2	3.6 ± 1.3, 42.6	1.4 ± 1.3, −100.3	1.5 ± 1.3, 4.9	0.6 ± 1.3, −132.6

Phase lags are negative. P_1 is not modelled directly in FES99. Also shown are the formal errors (one standard deviation) for the GPS-estimated amplitudes from both the kinematic and static analyses.

Table 2
Same as Table 1 but for the East component

Method	Constituent (East)							
	M_2	S_2	N_2	K_2	K_1	O_1	P_1	Q_1
TPXO.6	0.61, −63.2	0.28, 47.2	0.15, −90.2	0.07, 51.1	1.43, 149.2	1.43, 130.2	0.48, 150.7	0.32, 116.9
FES99	0.65, −59.8	0.32, 40.2	0.17, −84.5	0.08, 36.3	1.47, 147.6	1.40, 129.6	–	0.32, 113.2
Kinematic	0.6 ± 0.2, 28.3	0.4 ± 0.2, −49.1	0.1 ± 0.2, 25.6	0.2 ± 0.2, 155.1	2.2 ± 0.4, 115.2	1.4 ± 0.4, 158.1	0.3 ± 0.3, −112.9	0.3 ± 0.4, 142.5
Static	0.9 ± 0.6, 21.1	0.5 ± 0.6, −67.0	0.2 ± 0.6, −9.0	1.1 ± 0.6, 123.6	1.6 ± 0.6, 111.6	1.5 ± 0.6, 134.7	1.0 ± 0.6, −144.9	0.2 ± 0.6, 65.2
Static + PN	1.0 ± 0.7, 24.0	0.4 ± 0.8, −65.3	0.2 ± 0.7, −15.8	1.9 ± 4.8, −133.2	1.6 ± 0.6, 121.9	1.6 ± 0.6, 137.1	1.1 ± 0.6, −144.4	0.2 ± 0.6, 50.2

Table 3
Same as Table 1 but for the North component

Method	Constituent (North)							
	M_2	S_2	N_2	K_2	K_1	O_1	P_1	Q_1
TPXO.6	1.35, 98.5	0.35, 114.5	0.22, 64.7	0.10, 111.0	1.84, −136.9	1.92, −152.0	0.61, −138.2	0.42, −165.6
FES99	1.41, 98.6	0.36, 110.7	0.19, 63.6	0.11, 108.3	1.87, −137.3	1.92, −151.1	–	0.44, −166.0
Kinematic	0.7 ± 0.2, 118.1	0.7 ± 0.2, 185.1	0.2 ± 0.2, 95.8	0.8 ± 0.2, 83.7	0.3 ± 0.4, −122.7	1.9 ± 0.5, −161.9	2.1 ± 0.4, −141.1	0.5 ± 0.4, 170.1
Static	0.9 ± 0.7, 125.6	1.2 ± 0.6, 154.5	0.2 ± 0.7, 109.3	1.4 ± 0.6, 68.9	3.6 ± 0.6, −128.6	2.1 ± 0.6, −160.9	1.7 ± 0.6, −141.3	0.5 ± 0.6, −162.0
Static + PN	1.0 ± 0.7, 122.3	1.1 ± 0.8, 151.9	0.2 ± 0.7, 90.0	2.2 ± 5.0, 88.5	3.6 ± 0.6, −128.2	2.1 ± 0.6, −162.9	1.8 ± 0.6, −142.0	0.5 ± 0.6, −160.5

largest model differences are evident for N_2 and O_1 with vector differences close to 0.2 mm. Apart from these, the agreements are at the level of a few hundredths of 1 mm.

2.2. Kinematic GPS technique

King and Aoki (2003) showed that it is possible to measure ocean tide signals using only a single GPS receiver with the Precise Point Positioning GPS data processing approach (Zumberge et al., 1997). This technique allows the determination of site coordinates by fixing satellite orbit and clock and earth orientation parameters at values from an earlier global analysis. Site coordinates may be generated up to once per measurement epoch in a Kalman Filter (or similar), with the site motion constrained through the choice of filter process noise. Subsequent experience (e.g., Bindschadler et al., 2003) has shown that epoch-to-epoch repeatabilities are ∼0.02 and 0.05 m in the horizontal and vertical components respectively at high latitudes over snow/ice surfaces.

The same procedure was largely followed for the estimation of tidal displacement signals at AMUN using the GIPSY/OASIS software (Webb and Zumberge, 1995). Data between 1998.5 and 2003.5 was processed in 30 h batches and to reduce edge effects only the central 24 h retained. Fiducial satellite orbit and clock products from the Jet Propulsion Laboratory (JPL) were used. An elevation cut-off angle of 7° was used and Earth body tides modelled. Site motion was loosely constrained using a random walk standard deviation (Lichten, 1990) of 4.2 mm/$\sqrt{\text{h}}$, with tropospheric zenith delay (TZD) constrained at the level of 4.8 mm/$\sqrt{\text{h}}$. Horizontal tropospheric gradients were not estimated. Site coordinates were generated every 5 min following backward smoothing, although data was decimated to hourly intervals prior to tidal analysis (Pawlowicz et al., 2002).

All constituents that could be separated by at least one complete period from their neighbouring constituents over the length of data record (i.e., a Rayleigh criterion of 1 (Godin, 1972)) were solved in this analysis (68 in total), plus a linear drift to allow for vertical motion of the AMUN site. A different analysis solving for a reduced set of constituents gave only negligibly different results. Non-tidal (systematic or random) noise dominates the time series since tidal signals explained less than 0.1% of the time series variance. Constituent noise estimates were estimated using a coloured noise approach (Pawlowicz et al., 2002) and the vertical estimates are shown in Table 1. The level of agreement between the model and kinematic estimates is not uniform across constituents. For example, the M_2 estimate is almost an order of magnitude too small, even considering its uncertainty. The other constituents are in generally better agreement, although they often still differ given their uncertainties.

Solar-related constituents have the greatest signal-to-noise ratios (SNR) (defined as the square of the ratio of estimated amplitude to formal amplitude error from the harmonic analysis), with P_1, S_1, K_1, S_2 and K_2 having SNRs greater than 2. Of the lunar constituents, M_2 has a SNR of 1.1, with the remainder of the constituents having SNRs below 1. The dominance of the solar constituents is suggestive of GPS systematic effects, especially with the presence of a 1.5 mm S_1 signal, other than K_1 the largest amplitude determined. Given that S_1 ocean and atmospheric tide loading displacements are several orders smaller than 1 mm at this site (Ray and Egbert, 2004; Ray and Ponte, 2003), either diurnal tropospheric gradients, orbit mismodelling or second order ionospheric disturbances (Kedar et al., 2003) are the most likely sources of this signal. The failure of the approach to detect the ∼1.1 mm M_2 signal means that realistic uncertainty estimates for the constituents are at least comparable to the magnitude of the determined signals. On the other hand, the lack of wildly erroneous constituent estimates does show that a lower accuracy bound for the technique is approximately 1–2 mm.

The horizontal estimates are shown in Tables 2 and 3. The agreements between the models and the kinematic estimates are mixed, with the disagreement with M_2 again evident in the north component where the kinematic estimate is lower (as with the vertical estimate). Overall, the differences are generally larger than the kinematic estimate uncertainties.

2.3. Static GPS technique

Estimation of harmonic parameters in static GPS time series has been demonstrated by, for example, Allinson et al. (2004) and Schenewerk et al. (2001). The approach used in this study was similar to that of King et al. (2005), using GIPSY/OASIS to estimate parameters at eight tidal frequencies for each of three dimensions, using JPL non-fiducial orbits and clocks. The only difference was due to the high site velocity (∼0.03 m/day) which, if uncorrected, could bias the harmonic estimates (King, 2004). So, before analysis in GIPSY the horizontal velocity was first removed from

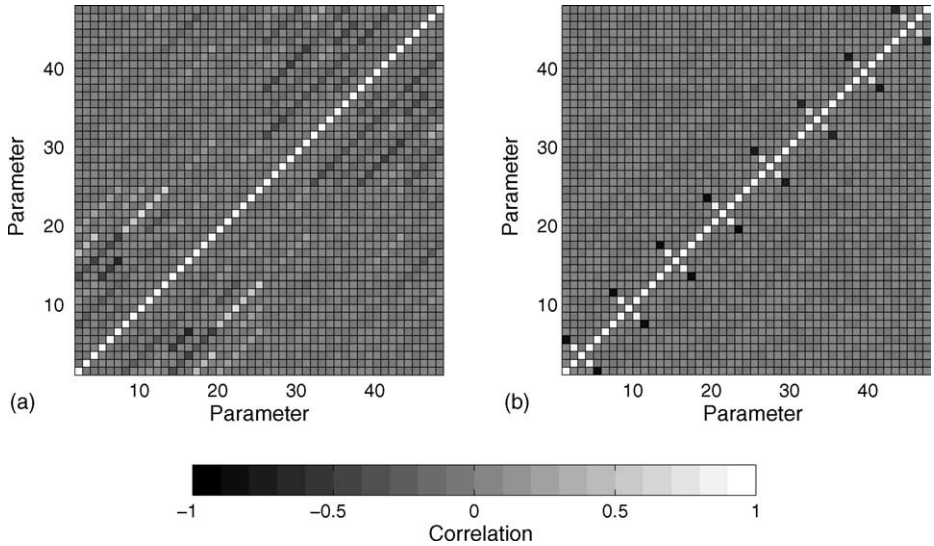

Fig. 1. AMUN harmonic parameter correlations (R) from one daily estimate (a) and after combination of all daily estimates (b). Parameter numbers 1–6 are the M_2 east, north, vertical cosine parameters, followed by the sine components. In the same way, these are followed by the parameters relating to S_2, N_2, K_2, K_1, O_1, P_1 and Q_1.

the daily RINEX files (King et al., 2000) using a velocity determined using a conventional multi-year PPP solution. The solutions shown here for AMUN are therefore an improvement on those shown in King et al. (2005). After this correction to the RINEX data the analysis continued in GIPSY. To overcome potential numerical instabilities due to the closeness of the tidal frequencies, constraints of 0.2 and 0.02 m were placed on each initial parameter estimate in the vertical and horizontal components, respectively. These constraints were chosen to be several times the largest possible constituent estimate, and hence do not overly constrain the estimates. An elevation cut-off angle of 7° was used and Earth body tides were modelled. Tropospheric zenith and horizontal gradient estimates were made at each measurement epoch (5 min after pseudorange smoothing and decimation), using random walk standard deviations of 10.2 and 0.3 mm/$\sqrt{\text{h}}$, respectively. The daily harmonic parameter estimates were then combined together with their variance–covariance information in a Kalman Filter with zero process noise (effectively a weighted average). The daily

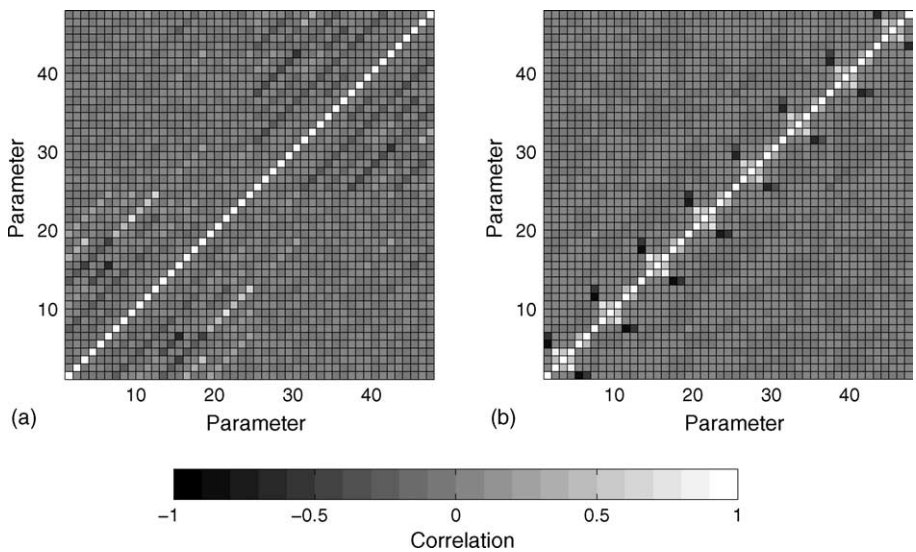

Fig. 2. Same as Fig. 1, but for CAS1 (66.3°S, 110.5°E).

unit variances were computed on the first iteration and on a subsequent iteration these were used to scale the daily variance–covariance matrices and obtain the final harmonic parameter estimates.

The parameter correlations (R) derived from the variance–covariance matrix for a single daily solution (harmonic parameters only) are shown in Fig. 1a. Examining R shows values greater than 0.5 between S_2 and K_2 for east, north and vertical, respectively. Since these constituents are the closest in frequency of those estimated (separated in period by only 0.03 h), a maximum R of 0.7 reflects that numerical stability of the daily solutions. Following the combination of all daily solutions between ~1998.5 and 2003.5, the values of R are as shown in Fig. 1b. The majority of the constituent estimates are now decorrelated, with $R < 0.06$. For each constituent however, the east cosine component is correlated with the north sine component and the north cosine component correlated with the east sine component, resulting in the pattern shown. These vary according to constituent species; for the diurnal constituents they are all close to 0.7 and for the semi-diurnal constituents they are close to 0.9. The existence of these correlations reflects the site latitude and GPS satellite constellation geometry since repeating these experiments at other latitudes produced a slightly different pattern to Fig. 1b, with increased correlations between the horizontal and vertical components (Fig. 2). While further investigation is required, these may be reflective of the presence of non-integer carrier phase ambiguities in the daily solutions. It has been previously demonstrated that choosing not to fix these parameters to integers may introduce correlations between the east and vertical (Blewitt, 1989; King et al., 2003), although different correlations occur at high latitudes (King, 2004).

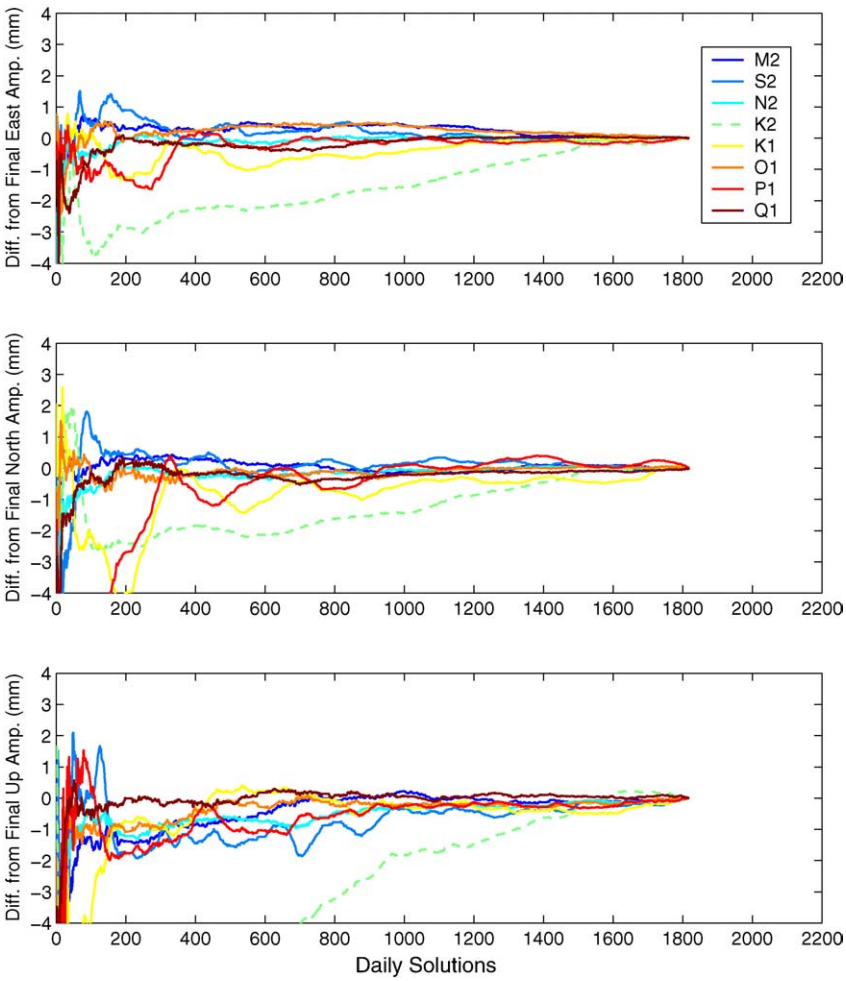

Fig. 3. Harmonic parameter amplitude estimates after the addition of each daily solution, relative to the final estimate, for east (top), north (middle) and vertical (bottom).

The vertical harmonic parameter estimates from the combined solution are shown in Table 1. The static estimates are closer to the model estimates than the kinematic estimates, with good agreement in phase. In fact, apart from K_1 and S_2, the phase obtained from the static GPS estimates are in agreement with the model estimates. Given the uncertainties on the static estimates, neither model is preferred for N_2 or O_1. The static S_2, K_2 and K_1 estimates are in worse agreement, having amplitude differences of >1 mm and as with the kinematic solutions their solar origin is suggestive of GPS-related systematic errors. The differences for O_1, P_1 and Q_1 are also systematically too large, although for O_1 and Q_1 these are within the uncertainties. The horizontal components (Tables 2 and 3) further confirm the generally closer agreement with the models than found when comparing the kinematic estimates.

As the daily solutions are combined together in a Kalman Filter, parameter estimates may be examined following the addition of each additional day of data. The time-variation of the parameter estimates is shown in Fig. 3, for amplitude and phase for each of the eight constituents, relative to the final estimates obtained after all data were added. The K_2 amplitude estimate does not stabilise during the period of the observations, whilst the other constituents obtain reliable estimates with ∼900 daily solutions. In comparison, Q_1 has a similar predicted amplitude to K_2 and it stabilises on its final estimate very quickly. The slow convergence rate in K_2 amplitude suggests a time-variable behaviour to this constituent with presently unknown origin, although it is presumably related to the changes in the GPS satellite constellation made up of satellites with an orbital period being nominally at this frequency.

The time-variable behaviour in K_2 will impact on the other constituents through their covariances. To assess the possible effect, the daily static solutions were recombined, but with the addition of 1 mm^2 process noise to each of the K_2 parameters. The results are shown in Table 1. Due to the process noise, the K_2 estimate follows the measurements more closely and hence its estimate changes significantly from the zero process noise solution, with a corresponding increase in its uncertainty. Of the other constituents, S_2 is altered by the greatest amount, with a 0.6 mm increase in amplitude, showing the effect of the S_2/K_2 covariance. Further tests using a 25 mm^2 process noise of K_2 yielded a further change in S_2 amplitude, although it still did not resemble the modelled estimates, possibly due to real solar-related variations being present in the GPS data.

3. Discussion and conclusions

I have shown that using either the static or kinematic estimation techniques tidal displacement parameters may be determined with an accuracy of ∼0.5–1.0 mm at the South Pole, apart from K_1 and K_2. The GPS data were not of sufficient precision to separate FES99 and TPXO.6 for the two constituents where they differed most (N_2 and O_1).

The time-variable nature of the daily K_2 estimates was also demonstrated and the addition of process noise to this parameter improved the agreement of S_2 with the model results, although unmodelled solar-related effects are evident in both the static and kinematic results. Changes in processing strategies at JPL during the period of the orbit computation may have an influence on K_2 over time, as would satellite-specific phase centre mismodelling such as shown by Ge et al. (2005). Tropospheric gradient parameters were not estimated in the kinematic solutions, and a spectral analysis of these parameters from the static solution suggested that this may be a source of some of the S_1 signal evident in the kinematic time series. The satellite products may have affected the relative accuracies of each of the respective techniques. Fiducial orbit and clock products were used in the kinematic analysis with fiducial-free products used in the static analysis, although the magnitude of this effect is not known. For the remainder, orbit mismodelling, multipath and higher-order ionospheric effects are likely sources of error, the later of which should be readily removed in the near future (Kedar et al., 2003). Ambiguity fixing is a further avenue for improving the static technique since this will decorrelate the three coordinate components which are presently strongly correlated.

Only the major semi-diurnal and diurnal constituents have been discussed in detail here. There are significant difficulties in estimating longer-period tidal signals such as M_f and M_m due to propagation of mismodelled shorter period signals using conventional analyses (Penna and Stewart, 2003). Both of the estimation strategies described here should allow the determination of longer period signals without the possibility of this problem. However, inspection of M_f and M_m estimates from the time series shows them to be accurate within 1–2 mm, although not significantly different from 0 (the modelled estimates are ∼1 mm). Before these may be determined much longer time series are required and the correction for other loading effects (e.g., atmospheric loading displacements) considered.

While the results shown here suggest GPS tidal displacement estimates are not yet as consistently accurate as those from VLBI, promised global navigation satellite system (GNSS) changes (the launch of the Galileo constellation and the replenishment of the GLONASS constellation) should in the future assist in the identification and removal of systematic

errors at tidal frequencies (due to their orbital periods being at non-tidal frequencies) and add extra observations to further reduce random errors. The extension of the GPS time series as new data are collected will further reduce the random errors and allow more accurate separation of tidal constituents. As a result, GNSS measurements of tidal displacements will increase in both accuracy and precision in the coming decades.

Acknowledgements

This work would not have been possible without the foresight of Larry Hothem (USGS) to install a GPS receiver at AMUN during the early 1990s. We also thank JPL for providing GPS orbits and clock products, Frank Wu for providing modified GIPSY routines and Duncan Agnew for making his SPOTL software freely available. I also thank Hans-Georg Scherneck, two further anonymous reviewers and Editor Rüdiger Haas for their comments which helped to significantly improve this paper.

References

Agnew, D.C., 1995. Ocean-load tides at the South Pole—a validation of recent ocean-tide models. Geophys. Res. Lett. 22 (22), 3063–3066.

Agnew, D.C., 1997. NLOADF: a program for computing ocean-tide loading. J. Geophys. Res. 102 (B3), 5109–5110.

Allinson, C.R., Clarke, P.J., Edwards, S.J., King, M.A., Baker, T.F., Cruddace, P.R., 2004. Stability of direct GPS estimates of ocean tide loading. Geophys. Res. Lett. 31, L15603, doi:10.1029/2004GL020588.

Bindschadler, R., King, M.A., Alley, R.B., Anandakrishnan, S., Padman, L., 2003. Tidally controlled stick-slip discharge of a West Antarctic ice stream. Science 301 (5636), 1087–1089.

Blewitt, G., 1989. Carrier phase ambiguity resolution for the Global Positioning System applied to geodetic baselines up to 2000 km. J. Geophys. Res. 98 (B8), 10187–10203.

Egbert, G.D., Bennett, A.F., Foreman, M.G.G., 1994. TOPEX/POSEIDON tides estimated using a global inverse model. J. Geophys. Res. 99 (C12), 24821–24852.

Egbert, G.D., Erofeeva, S.Y., 2002. Efficient inverse modeling of barotropic ocean tides. J. Atmos. Ocean. Technol. 19 (2), 183–204.

Fricker, H.A., Allison, I., Craven, M., Hyland, G., Ruddell, A., Young, N., Coleman, R., King, M., Krebs, K., Popov, S., 2001. Redefinition of the Amery Ice Shelf, East Antarctica, grounding zone. J. Geophys. Res. 107 (5), doi:10.1029/2001JB000383.

Ge, M., Gendt, G., Dick, G., Zhang, F.P., Reigber, C., 2005. Impact of GPS satellite antenna offsets on scale changes in global network solutions. Geophys. Res. Lett. 32 (6), art. no. L06310.

Godin, G., 1972. The Analysis of Tides. University of Toronto Press, Toronto, p. 264.

Hinderer, J., Crossley, D., 2004. Scientific achievements from the first phase (1997–2003) of the Global Geodynamics Project using a worldwide network of superconducting gravimeters. J. Geodynam. 38 (3–5), 237–262.

Kedar, S., Hajj, G.A., Wilson, B.D., Heflin, M.B., 2003. The effect of the second order GPS ionospheric correction on receiver positions. Geophys. Res. Lett. 30 (16.), 1829, doi:10.1029/2003GL017639.

Khan, S.A., Scherneck, H.G., 2003. The M_2 ocean tide loading wave in Alaska: vertical and horizontal displacements, modelled and observed. J. Geod. 77 (3–4), 117–127, doi:10.1007/s00190-003-0312-y.

Khan, S.A., Tscherning, C.C., 2001. Determination of semi-diurnal ocean tide loading constituents using GPS in Alaska. Geophys. Res. Lett. 28 (11), 2249–2252.

King, M., 2004. Rigorous GPS data processing strategies for glaciological applications. Journal of Glaciology 50 (171), 601–607.

King, M., Aoki, S., 2003. Tidal observations on floating ice using a single GPS receiver. Geophys. Res. Lett. 30 (3), 1138, doi:10.1029/2002GL016182.

King, M., Coleman, R., Morgan, P., 2000. Treatment of horizontal and vertical tidal signals in GPS data: a case study on a floating ice shelf. Earth Planets Space 52 (11), 1043–1047.

King, M., Coleman, R., Nguyen, L., 2003. Spurious periodic horizontal signals in sub-daily GPS position estimates. J. Geod. 77 (1–2), 15–21, doi:10.1007/s00190-002-0308-z.

King, M.A., Penna, N.T., Clarke, P.J., King, E.C., 2005. Validation of ocean tide models around Antarctica using onshore GPS and gravity data, J. Geophys. Res. 110, B08401, doi:10.1029/2004JB003390.

Knopoff, L., Rydelek, P.A., Zurn, W., Agnew, D.C., 1989. Observations of load tides at the South-Pole. Phys. Earth Planet. Interiors 54 (1–2), 33–37.

Lambert, A., Pagiatakis, S.D., Billyard, A.P., Dragert, H., 1998. Improved ocean tide loading corrections for gravity and displacement: Canada and northern United States. J. Geophys. Res.—Solid Earth 103 (B12), 30231–30244.

Lefevre, F., Lyard, F.H., Le Provost, C., Schrama, E.J.O., 2002. FES99: a global tide finite element solution assimilating tide gauge and altimetric information. J. Atmos. Ocean. Technol. 19 (9), 1345–1356.

Lichten, S.M., 1990. Estimation and filtering for high-precision GPS positioning applications. Manuscripta Geod. 15, 159–176.

Pawlowicz, R., Beardsley, B., Lentz, S., 2002. Classical tidal harmonic analysis including error estimates in MATLAB using T_TIDE. Comput. Geosci. 28 (8), 929–937.

Penna, N.T., Stewart, M.P., 2003. Aliased tidal signatures in continuous GPS height time series. Geophys. Res. Lett. 30 (23), 2184, doi:10.1029/2003GL018828.

Petrov, L., Ma, C.P., 2003. Study of harmonic site position variations determined by very long baseline interferometry. J. Geophys. Res. 108 (B4), 2190, doi:10.1029/2002JB001801.

Ray, R.D., Egbert, G.D., 2004. The global S-1 tide. J. Phys. Oceanogr. 34 (8), 1922–1935.
Ray, R.D., Ponte, R.M., 2003. Barometric tides from ECMWF operational analyses. Ann. Geophys. 21, 1897–1910.
Schenewerk, M.S., Marshall, J., Dillinger, W., 2001. Vertical ocean-loading deformations derived from a global GPS network. J. Geod. Soc. Jpn. 47 (1), 237–242.
Schuh, H., Moehlmann, L., 1989. Ocean loading station displacements observed by VLBI. Geophys. Res. Lett. 16 (10), 1105–1108.
Sovers, O.J., 1994. Vertical ocean loading amplitudes from VLBI measurements. Geophys. Res. Lett. 21 (5), 357–360.
Vey, S., Calais, E., Llubes, M., Florsch, N., Woppelmann, G., Hinderer, J., Amalvict, M., Lalancette, M.F., Simon, B., Duquenne, F., Haase, J.S., 2002. GPS measurements of ocean loading and its impact on zenith tropospheric delay estimates: a case study in Brittany, France. J. Geod. 76 (8), 419–427.
Webb, F.H., Zumberge, J.F., 1995. An Introduction to GIPSY/OASIS-II Precision Software for the Analysis of Data from the Global Positioning System. Jet Propulsion Laboratory, Pasadena, CA.
Zumberge, J.F., Heflin, M.B., Jefferson, D.C., Watkins, M.M., Webb, F.H., 1997. Precise point positioning for the efficient and robust analysis of GPS data from large networks. J. Geophys. Res. 102 (B3), 5005–5017.